Jo et al. Int J Concr Struct Mater (2025) 19:71
https://doi.org/10.1186/s40069-025-00813-0

International Journal of Concrete Structures and Materials

RESEARCH Open Access

Proposal for Bond Strength Considering Bond Characteristics of Beam Flexural Rebar on Interior Beam-Column Joints. Part I: Focusing on Concrete Compressive Strength

Min-Su Jo[1], Hyeong-Gook Kim[2], Dong-Hwan Kim[3], Su-A Lim[3], Yun-Soo Choi[4], Jung-Yoon Lee[5] and Kil-Hee Kim[6*]

Abstract

The bond characteristic of beam longitudinal rebar penetrating reinforced concrete beam-column interior joints under cyclic loading is influenced by various factors such as compressive strength of concrete, yield strength of main rebar, diameter, and axial load ratio of column. In this study, the bond characteristics of beam longitudinal rebar were investigated through an experimental method that directly simulates the internal stress state of the joint; a bond strength equation reflecting the bond behavior focused on the concrete compressive strength was proposed. The experiments were conducted by fabricating eight specimens with concrete compressive strength as the main variable and performing cyclic loading tests. Through the experimental results, it was confirmed that the mechanism of bond failure of beam longitudinal rebar penetrating into the joint is one in which bond stress in the tensile region results in degradation of the joint core region; the burden of bond stress increases due to transfer to the compression region; finally, bond failure of the joint core region occurs due to degradation of bond stress in the compression region. Based on the experimental results, the proposed bond strength equation, which reflects the bond characteristics of longitudinal reinforcement at the internal joint, is proportional to the 3/4 power of the concrete compressive strength, and shows a prediction result that is about 5–16% better than that of the existing design equation. In addition, in order to propose the required column depth, it is necessary to consider various parameters such as the column axial force ratio, yield strength of beam longitudinal rebar, and diameter.

Keywords RC interior beam-column joint, Penetrated beam rebar, Concrete compressive strength, Bond characteristics, Bond strength

*Correspondence:
Kil-Hee Kim
kimkh@kongju.ac.kr
Full list of author information is available at the end of the article

1 Introduction and Background

Under seismic loading, the stability and seismic performance of reinforced concrete (hereinafter, RC) structures are highly dependent on how the various elements of the structure interact. In particular, RC moment-resisting frames are widely used as structural systems that play important roles in the absorption and dissipation of seismic energy (Sadjadi et al., 2007). In such framing systems, beam-column joints are key elements that transfer loads acting on upper columns to lower columns, anchor main reinforcement of beams, and distribute external forces according to stiffness of beams and columns. In addition, the beam-column joint is subject to shear and bond forces that are much greater than flexural moments, and there is a risk of the entire floor collapsing due to brittle failure (shear, bond) (Alva et al., 2007; Hong et al., 2011; Karayannis & Chalioris, 2013; Lee et al., 1992; Meinheit & Jirsa, 1977).

Figure 1 shows the load transfer mechanism of RC interior beam-column joints during seismic loading (hereafter, cyclic loading). Under cyclic loading, the shear force and flexural moment generated in the beam cause the beam rebar to generate not only tensile force (T_1, T_2) but also compressive force (C_1, C_2). Therefore, in principle, under cyclic loading, twice the bond stress (T_1+C_2 or T_2+C_2) is generated at the joint compared to the case of monotonic loading. On the other hand, the maximum development length of the beam main rebar at the joint is limited to the section depth of the column, h_c, which makes it difficult to secure sufficient development performance. According to previous studies, the behavior of beam-column joints depends on the ratio (h_c/d_b) of the depth of the column's cross-section (h_c) to the diameter of the rebar (d_b) that penetrates the joint (Brooke et al., 2006; Hakuto et al., 1999; Kitayama et al., 1987; Leon, 1989). Therefore, when h_c/d_b is small, bond failure occurs in the joint region, which leads to an increase in deformation due to slippage of the reinforcing bar in the joint region, which reduces the performance. As a result, there is a risk that the diagonal cracks in the concrete may be enlarged in the joint area and concrete failure may occur prematurely. In addition, as shown in Fig. 2, at both ends of the joint, tensile stress (f_s) and compressive stress (f'_s) are generated in the beam's main rebar due to the flexural moment of the beam, and bond stress (τ_f) is generated inside the joint to achieve equilibrium. The bond stress (τ_f) that occurs at this time can be shown by Eq. (1).

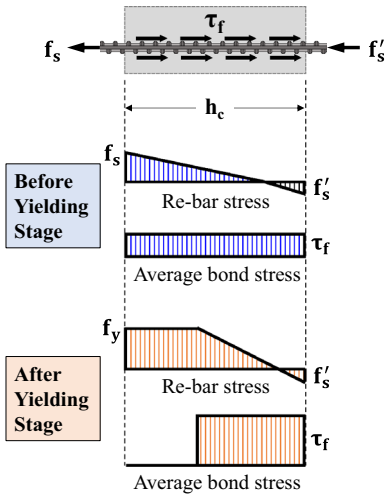

Fig. 2 Bond stresses of rebar in joint

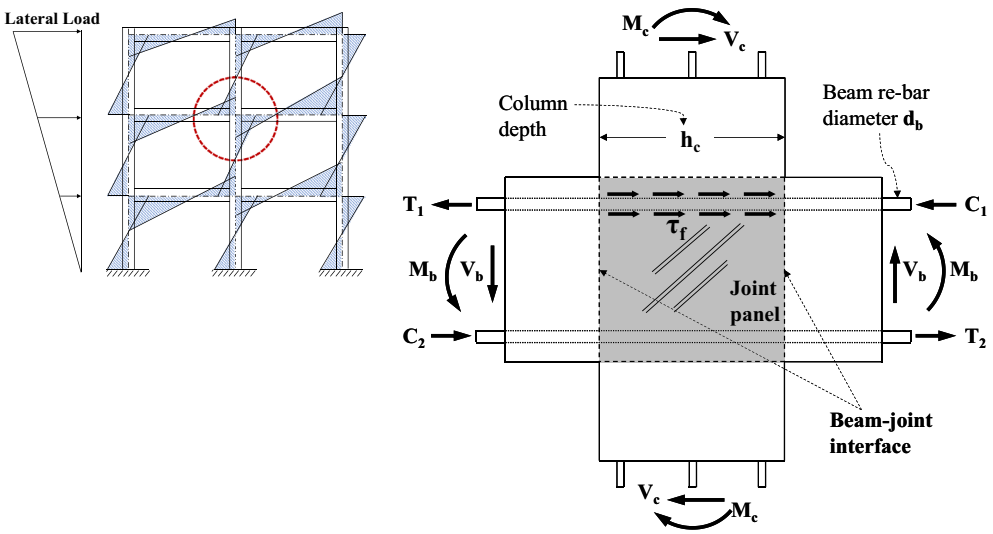

Fig. 1 Load transfer mechanism of interior beam-column joint

$$\tau_f = \frac{(f_s + f_s')d_b}{4h_c} \quad (1)$$

After reaching the plastic hinge of the beam (see Fig. 2(b)), the yield strain of the reinforcing bars penetrates into the joint (Lee et al., 2009) and, as a result, the bond stress (τ_f) inside the joint increases even more than before the plastic hinge (Fig. 2(a)) than before the occurrence of plastic hinge, requiring an increase in the column section depth (h_c). To suppress the risk of bond failure at beam-column joints, existing design criteria limit the bond strength (τ_u) and the corresponding required column width ($h_{c,req}$) considering the influence of concrete compressive strength at interior joints in seismic design, as shown in Table 1. ACI 318–19 (ACI 2019) and NCREE-19–001 (NCREE 2019) simply define h_c/d_b based on the yield strength of the reinforcement bar, and do not provide an expression for the bond strength (τ_u). AIJ (2010) (AIJ 2010) and NZS 3101 (2006) (NZS, 2006) provide a bond strength expression (τ_u) based on the compressive strength of concrete and consider design variables such as column axial load ratio and required seismic performance in addition to h_c/d_b.

As an experimental and theoretical study, Fujii et al. (1991) modeled beam longitudinal rebar passing through an interior beam-column joint to evaluate the bond characteristic. They proposed an equation for predicting the bond strength through various variables such as beam longitudinal rebar diameter, yield strength, concrete compressive strength, and axial load ratio, and provided the basis for the criteria for the required column depth in AIJ (2010) (AIJ 2010). Hwang et al. (2015) developed a simplified bond model that can consider the slip of rebar in beam-column joints subjected to cyclic loads, and evaluated model suitability with experimental data of existing joint members. However, the simplified bond model was proposed based on the theoretical background and does not reflect the bond characteristic considering the stress state of actual beam-column joints. Lee et al. (2018) proposed a simplified design equation for the required column width in special moment framing. The proposed equations were evaluated based on an experimental database of conventional beam-column joints with main reinforcement yield strengths of 490 MPa, 590 MPa, and 690 MPa. The proposed design equation was simplified based on the existing design equation, but it has limitations because it does not reflect the experimental data considering the bond characteristic of actual joints. In the study of Lee et al. (2009), the influence of strain penetration phenomenon on the potential shear strength of the joint after yielding of beam longitudinal rebar under cyclic loading was evaluated. It was found that the strain in the beam longitudinal rebar inside the joint, measured through an internal beam-column joint test, penetrated into the joint after yielding, and the shear strength of the joint was reduced due to this effect.

2 Research Significance

In this study, a bond test method that directly simulates the stress state inside the joint was proposed to check the bond characteristic of beam longitudinal rebar at interior beam-column joints, and experiments were conducted accordingly. Based on the experimental results, the bond characteristic of penetrating inside the joint beam longitudinal rebar and concrete was directly determined, and the influence of concrete compressive strength on the bond characteristic of beam longitudinal rebar was evaluated. Furthermore, a bond strength equation for beam longitudinal rebar that considers the bond characteristic focused on concrete compressive strength was proposed.

Table 1 Comparison of existing design equations for required column depth

Design criteria	Basic bond strength (τ_u)	Require column depth ($h_{c,req}$)
ACI 318–19	–	$\frac{h_{c,req}}{d_b} \geq 20, \left(atf_y \leq 400MPa\right)\ \frac{h_{c,req}}{d_b} \geq 25, \left(atf_y > 400MPa\right)$
AIJ (2010)	$0.7 f'^{\frac{2}{3}}_C$	$\frac{d_b}{h_{c,req}} \leq \frac{2.8}{1+\gamma}\left(1+\frac{f_0}{f'_c}\right)\frac{f'^{\frac{2}{3}}_C}{f_{yu}}$
NCREE-19–001	–	$Max\left(h_{c,req} = \frac{\alpha_0 f_y}{4\sqrt{f'_c}} d_b, h_{c,req} = 20d_b\right)$
NZS 3101 (2006)	$\alpha_f \alpha_t 1.5\sqrt{f_C}'$	$\frac{d_b}{h_{c,req}} \leq 6\left(\frac{\alpha_t \alpha_p}{\alpha_s}\right)\alpha_f \alpha_d \frac{\sqrt{f'_c}}{1.25 f_y}$

d_b = diameter of beam longitudinal rebar; f_y = yield strength of beam longitudinal rebar; f'_c = concrete compressive strength; γ:beam reinforcement ratio; f_0 = compressive stress of column; f_{yu} = ultimate strength of beam longitudinal rebar; α_0 = bar overstrength factor; α_f = 0.85 for bi-directional loading; α_t = 0.85 for a top beam bar for which more than 300 mm of fresh concrete is cast below the bar; α_t = 1.0 for all other cases; α_p = factor for column axial stress on bond; α_s = factor for bar stresses at joint faces; α_d = facto related to beam plastic regions

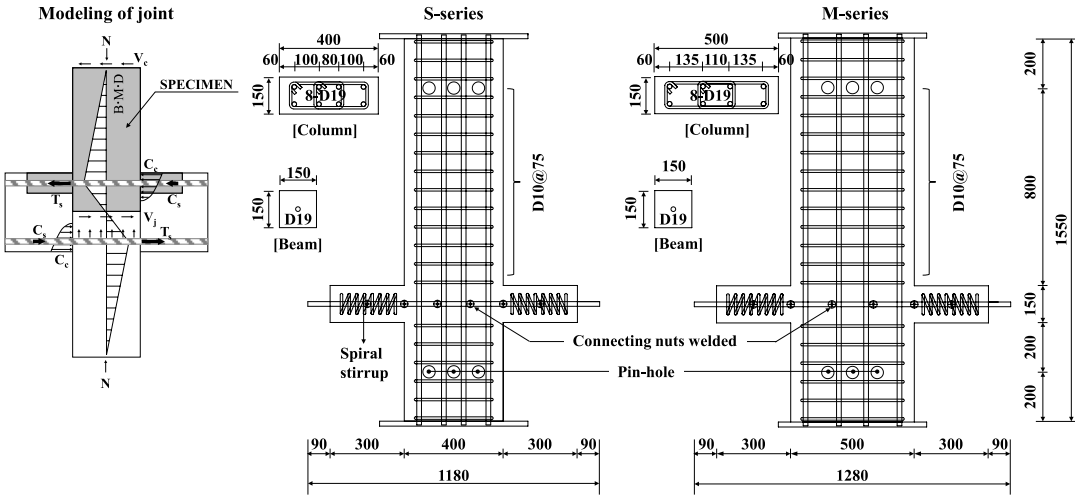

(a) Reinforcing details of specimens (unit: mm)

(b) Beam longitudinal re-bar

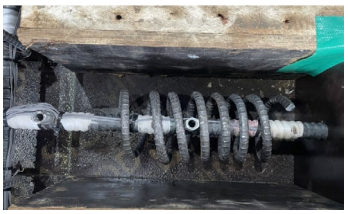

(c) Detail of spiral stirrup

(d) Photo of Pin-hole

Fig. 3 Details of specimen

3 Experimental Investigation

3.1 Description of Specimens

In this study, a specimen was designed to simulate the stress state of a real interior beam-column joint. The stress state of the top beam longitudinal rebar at the beam-column joint under cyclic load was considered as shown in Fig. 3(a). As shown in the shaded part of Fig. 3(a), the specimen includes a column and a part of a beam, including the joint. The beam part includes concrete blocks in the area corresponding to the compression zone of the plastic hinge, and the beam longitudinal rebar (experimental rebar) is designed to penetrate inside the joint and expose a part of it to the outside. The width of the column (B_c) was designed to be the same as the beam width (B_b) corresponding to one penetrated rebar, and a total of eight specimens were manufactured by categorizing the specimens into S and M series based on the depth of the column (h_c, the bond length of the experimental rebar).

Details of the reinforcement of test specimens are shown in Fig. 3(b). For all the tests, the columns were reinforced with 8-D19 (SD400) bars in the main reinforcement and D10 (SD400) bars in the transverse reinforcement at 75 mm intervals in the outer and center parts of the main reinforcement. Three pin-holes were installed in the upper and lower of the columns prior to pouring for the installation of the prestressing frame (see Fig. 3(d)). The cross-section of the concrete block corresponding to the plastic hinge of the beam was 150 × 150 mm for all test specimens, and one D19 rebar was placed to penetrate the center of the beam. In addition, a total of four connecting nuts were welded at regular intervals at the position corresponding to the joint of the beam rebar, as shown in Fig. 3(a, b). The length of the concrete block was set to 300 mm from the column surface, and D10 spiral steel bars (SD400) were placed at 30 mm intervals to prevent premature compression, splitting, and bond failure (Fig. 3(c)).

Table 2 shows the list of test subjects. The test specimens were categorized into S-series (h_c = 400 mm) and M-series (h_c = 500 mm) based on the column depth (h_c). For each series, the concrete compressive strength (design strength f'c = 24, 30, 50, 70 MPa) was set as a detailed variable and the beam reinforcement (S-series: SD400, M-series: SD600) and axial load ratio (N/Agf'c = 0.1) of column were set to be the same. The concrete was poured with the column side (column depth direction) as the top, and the same

Table 2 Specifications of specimens

Speci-mens	f_c' (MPa)	Beam			Column					$\frac{N}{A_g f_c'}$
		Longitudinal rebars		Section (mm × mm)	Longitudinal rebars		Hoop rebars		Section (mm × mm)	
		f_{by} (MPa)	n_b		f_{cy} (MPa)	n_c	f_{hy} (MPa)	n_h		
S-24	25.1	439	1-D19	150 × 150	426	8-D19	457	D10@75	400 × 150	0.1
S-30	27.9	439	1-D19	150 × 150	426	8-D19	457	D10@75	400 × 150	0.1
S-50	51.0	439	1-D19	150 × 150	426	8-D19	457	D10@75	400 × 150	0.1
S-70	65.0	439	1-D19	150 × 150	426	8-D19	457	D10@75	400 × 150	0.1
M-24	25.1	628	1-D19	150 × 150	426	8-D19	457	D10@75	600 × 150	0.1
M-30	27.9	628	1-D19	150 × 150	426	8-D19	457	D10@75	600 × 150	0.1
M-50	51.0	628	1-D19	150 × 150	426	8-D19	457	D10@75	600 × 150	0.1
M-70	65.0	628	1-D19	150 × 150	426	8-D19	457	D10@75	600 × 150	0.1

f_{by} = yield strength of longitudinal rebar of beam; n_b = size of longitudinal rebar in beam; f_{cy} = yield strength of longitudinal rebars of column; n_c = size of longitudinal rebars in column; f_{hy} = yield strength of hoop rebar in column; n_h = size of hoop bar; $N/(A_g f_{ck})$ = axial load ratio of column

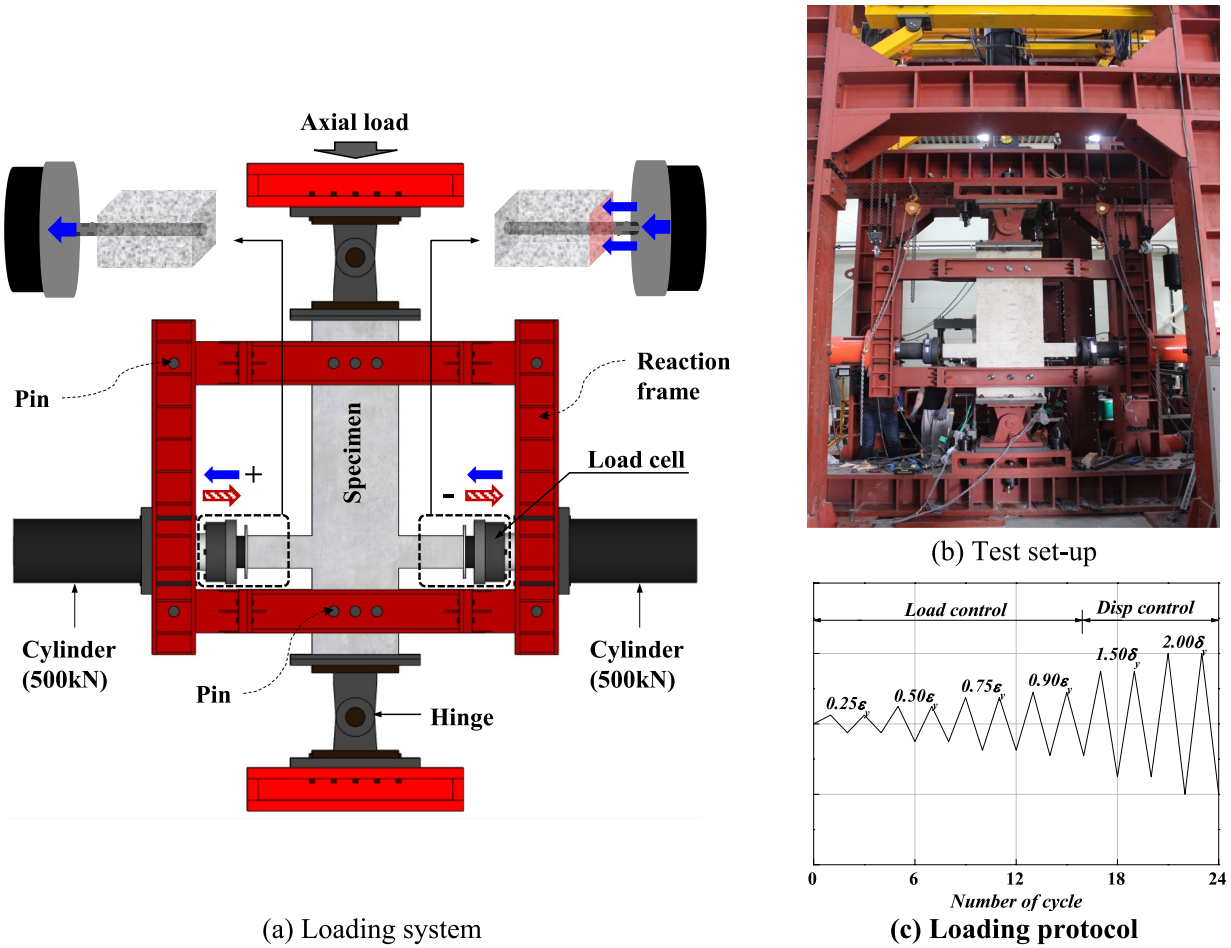

Fig. 4 Loading system, protocol, and test set-up

batch of ready-mixed concrete was used in each case. Concrete cylinders were made at the same time as the concrete was poured, and compressive strength tests (ASTM, 2021) were conducted before and after the test. The average values are shown in the second column of Table 2. The steel bars applied to the reinforcement were subjected to tensile tests; the results are shown in the 3rd, 6th, and 8th columns of Table 2. Meanwhile, the yield strength (f_y) values of SD400 and SD600 of D19, the beam longitudinal rebar, were 439 MPa and 628 MPa, respectively, and the yield strains (ε_y) were 2400 με and 4100 με, respectively.

3.2 Test Setup, Loading Protocol, and Measurement Methods

Figure 4 shows the load-bearing system of the test specimen and the experimental setup. The experiments were conducted using a structural fatigue testing machine (Smart Natural Space Research Center at Kongju National University). As shown in Fig. 4 (b), the upper and lower ends of the column were fixed using prefabricated hinges. Then, a horizontal frame was installed in the pin-holes at the top and bottom of the column, and a vertical frame with a 500 kN cylinder was connected and fixed to the horizontal frame with pins. The column axial load was applied using a 1,000 kN actuator attached to the top. Beam loading was applied by fixing a load cell connected to a cylinder to the longitudinal rebar of the beam exposed to the outside, and directly using a tensile load to the longitudinal rebar on one side, while applying an equivalent compressive load to the concrete block face on the opposite side together with the reinforcing bar. This method of loading reproduces a stress state of the beam longitudinal rebar similar to that of the interior beam-column joint. The loading protocol was based on the yield strain of the beam longitudinal rebar (ε_y described in the measurement method) and applied a load control method with two cycles of $0.25\varepsilon_y$, $0.5\varepsilon_y$, $0.75\varepsilon_y$, and $0.9\varepsilon_y$. After the reinforcing bar yielded, the load control method was changed to the displacement control method and the experiment was terminated after 2 cycles at $1.5\delta_y$ and $2.0\delta_y$ based on the displacement value (δ_y) at yield.

In this study, the measurement method shown in Fig. 5 was applied to quantitatively evaluate the bond stress and slippage of the beam longitudinal rebar. A total of 12 strain gauges (WSG) were attached to the experimental section to measure the bond stress of the reinforcing bars (Fig. 5 (a)). As explained above, the yield strain applied during the load control was calculated using the WSG of J1 and J6. J2 ~ J5 were attached to check the bond stress in the core region of the joint by zone (zones 1, 2, and 3) (Fig. 5 (a)). In addition, to measure the slip of the rebar, a stud bolt was connected using a connecting nut attached to the steel bar during test specimen fabrication as shown in Sect. 2.1. After that, the amount of slip was measured using a total of four linear variable differential transformers (LVDTs) installed on the outside of the specimen. To check the slip amount by section (local CL, CR, global), LVDT (CL, CR) was attached for measurement (Fig. 5 (a)). For displacement control after the yield point of the steel bar, a tie-down was used on the cylinder connected to the vertical frame.

4 Experimental Results

4.1 Crack Patterns and τ-Slip Relationship

Crack behaviors of S-24 and S-70 specimens are shown in Fig. 6. Due to the allowance of the thickness of the sheathing wrapped around the beam longitudinal rebar, no significant cracks were observed on the surface, but the bond characteristic of the beam longitudinal rebar can be measured using WSG and LVDT. In the figure, the cracks colored blue represent the crack distribution in the forward direction, while the cracks colored red represent the crack distribution in the backward direction. At the initial stage of loading ($0.25\varepsilon_y$), both S-24 and S-70

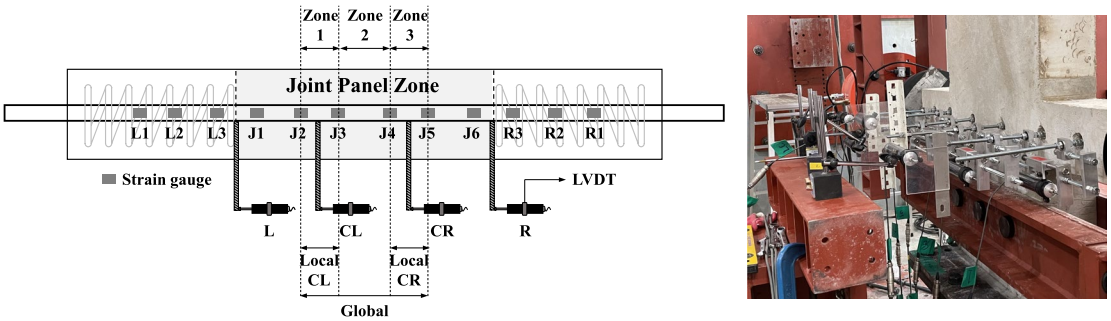

(a) Location map of strain gauge and LVDT

(b) LVDT setup

Fig. 5 Measurement methods

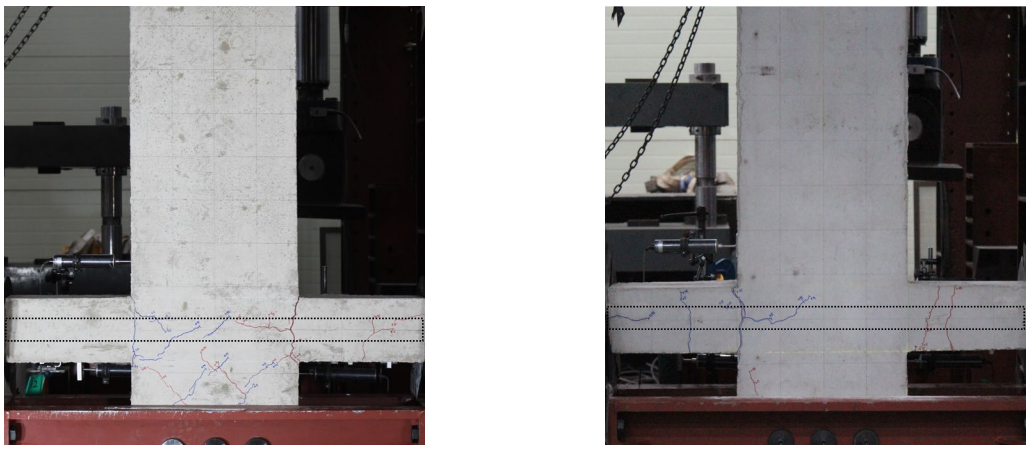

(a) S-24 (b) S-70

Fig. 6 Comparison of representative crack patterns at failure

specimens developed cracks in the concrete near the column boundary. Then, as the load increased, the S-24 specimen exhibited crack propagation from the tensile to the compressive side along the beam longitudinal rebar (solid line) in both the forward and reverse directions. In contrast, specimen S-70 showed crack propagation from the tensile side to the compressive side along the reinforcing bar in the forward direction, but no cracks occurred in the reverse direction.

Additionally, to compare the bond characteristics of each specimen, the relationship between bond stress (τ) and slippage amount (Slip) is shown in Fig. 7. The τ-Slip relationship was checked in three sections, focused on the core zone of the joint panel. At the initial stage of loading, LVDTs L and R and strain gauges J1 and J6 were excluded due to the influence of vertical cracks in the concrete block located at the boundary of the column, as shown in the crack pattern. The amount of bond stress and slip in the figure were calculated using the values measured by strain gauges and LVDTs attached to the beam longitudinal rebar, as shown in Eqs. (2) and (3) (see Fig. 5(a)). In Eq. (3), $Slip_{LVDT}$ represents the slip value of the longitudinal reinforcement, and Slippage (SLIP) represents the value of $Slip_{LVDT}$ excluding length increase due to deformation of longitudinal reinforcement.

$$\tau = \frac{(\varepsilon_{s1} + \varepsilon_{s2})A_{st}E_s}{\psi l_s} \tag{2}$$

$$\mathrm{SLIP} = Slip_{LVDT} - l_s(\varepsilon_{s1} - \varepsilon_{s2}) \tag{3}$$

Here, ε_{s1}, ε_{s2} = longitudinal reinforcement strain of test area for bond stress measurement; A_{st} = area of longitudinal reinforcement; E_s = elastic modulus of longitudinal reinforcement; ψ = nominal circumference of longitudinal reinforcement; l_s = length from ε_{s1} to ε_{s2}.

As described in Sect. 3.2, to check the bond characteristics in the core region of the joint in detail, the SLIP is divided into Local CL and Local CR, and the corresponding bond stresses are the bond stresses calculated in zone 1 and zone 3. The SLIP in the global section was calculated using the average value of LVDT CL and CR. As shown in Fig. 5(a), the WSG J2 ~ J5 section was defined as the joint core region (Global) in the joint panel area where the beam longitudinal rebar had penetrated. The local area was defined as the area subjected to tension and compression under cyclic loading in the joint core area based on LVDT CL and CR.

Figure 7 (a), (a-1), (a-2), and Table 3 show the relationship between the bond stress and slippage for each section of the S-30 specimen. As shown in Fig. 7 (a-1), the bond stress of the local CL reached the maximum bond stress (5.92 MPa) at $0.5\varepsilon_y$ during positive direction load; then, bond stress decreased during the next cycle at $0.75\varepsilon_y$. The bond stress in the local-CR area reached its maximum (8.87 MPa) at $0.75\varepsilon_y$; the bond stress in the global area reached the maximum point in the same cycle. After that, the bond stress decreased in the yield cycle ($0.9\varepsilon_y$). Based on the results of these experiments, the bond stress in the core area of the joint first degrades in the tensile area (Local CL) and then transfers to the compressive area (Local CR), increasing the share of the bond stress. Finally, the global core area's bond stress is degraded due to the degradation of the bond stress in the compression area. This phenomenon was also observed in the negative direction of the applied load, but the maximum bond stress was reached at a lower load cycle due to the influence of the preceding positive direction

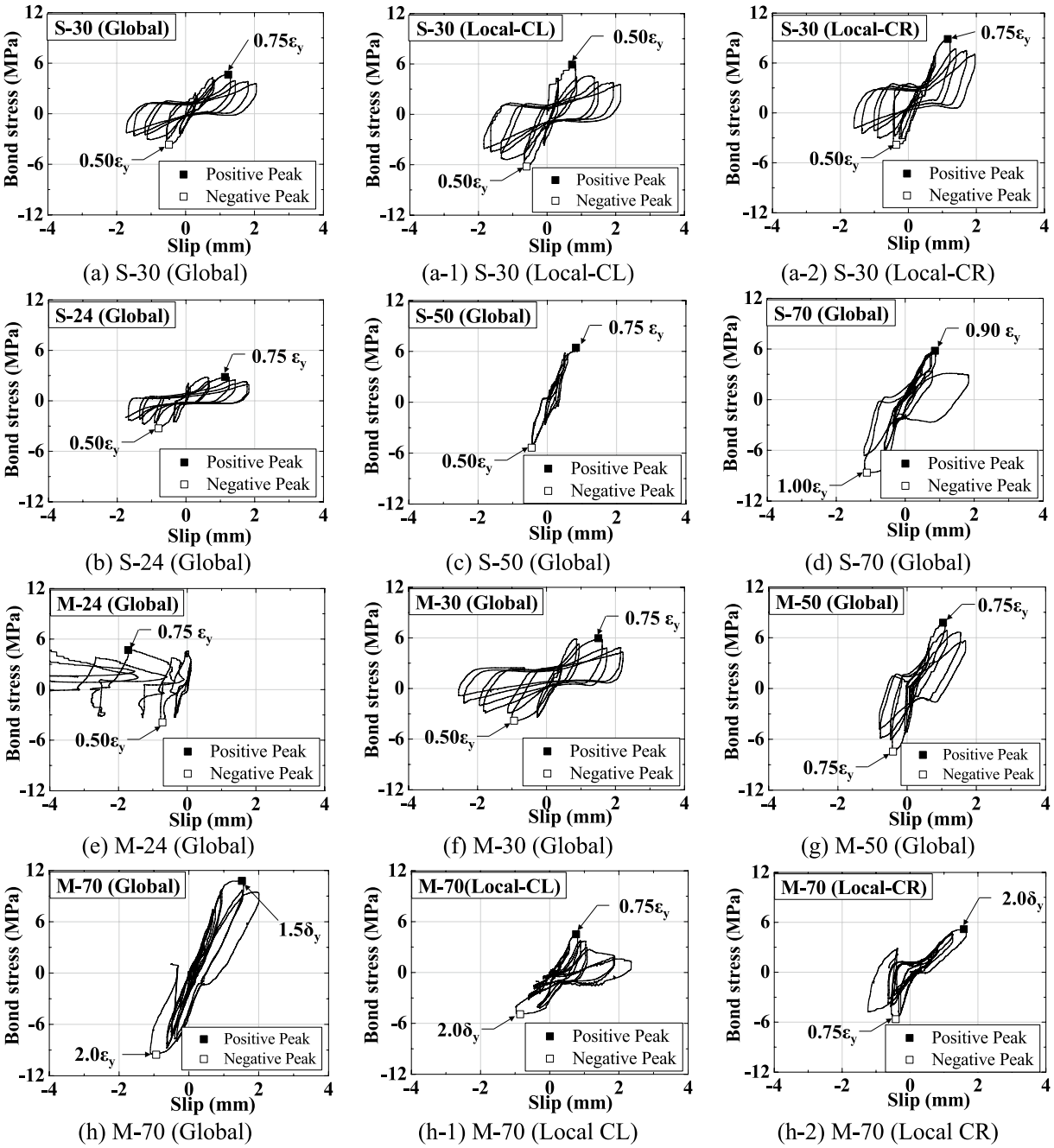

Fig. 7 Bond stress-slip relationship

of applied load. In addition, after reaching the maximum bond stress in each section, the amount of slip increased significantly, resulting in a pinching phenomenon, as confirmed in previous studies (Kitayama et al., 1987). This phenomenon was also observed in the same way at relatively low concrete strengths, as shown in Fig. 7 (b), (e), (f), and (g).

On the other hand, the bond stress-slippage relationship of the M-70 specimen in Fig. 7 (h), (h-1), (h-2) showed a different trend from that of the S-30 specimen. In the local CL, the maximum bond stress was reached at $0.75\varepsilon_y$ when load was applied in the positive direction; it degraded in subsequent cycles. On the other hand, the Local CR showed a healthy state without any degradation of the adhesive stress even after 0.75εy cyclic loading. In

Table 3 Amount of bond stress and slippage at peak for each region (positive direction)

Specimens	Local CL			Local CR			Global		
	Peak (ε_y)	τ_{CL} (MPa)	S_{CL} (mm)	Peak (ε_y)	τ_{CR} (MPa)	S_{CR} (mm)	Peak (ε_y)	τ_{Global} (MPa)	S_{Global} (mm)
S-24	0.25	1.07	0.08	0.75	4.98	1.12	0.75	2.84	1.13
S-30	0.50	5.92	0.72	0.75	8.87	1.15	0.75	4.63	1.23
S-50	0.50	1.04	0.47	0.70	7.71	0.76	0.75	6.43	0.81
S-70	0.75	5.07	0.63	0.90	5.16	0.66	0.90	5.79	0.85
M-24	0.25	1.91	–	0.75	7.71	–	0.75	4.68	–
M-30	0.50	5.29	0.61	0.50	5.13	0.89	0.75	5.95	1.49
M-50	0.50	5.50	0.67	0.75	5.96	0.95	0.75	7.76	1.02
M-70	0.75	4.50	0.76	2.00	5.17	1.58	1.50	10.77	1.50

the global area, the longitudinal rebar showed a healthy state without a decrease in the bond stress before yielding, and no pinching phenomenon was observed because there was no increase in the slip amount. This is thought to be because the use of high-strength concrete did not degrade the bond stress in the compression zone. This phenomenon can also be observed in Fig. 7 (c) and (d).

4.2 Strain and Bond Stress Distribution of Beam Longitudinal Rebar

The strain distribution of longitudinal reinforcing bars under positive direction of applied load is shown in Fig. 8. The strain rate distribution showed strain rate corresponding to the first cycle of each loading cycle in the panel area of the joint. In general, all test specimens showed a strain distribution in the form of a constant slope from the tensile side (J1) to the compression side (J6) at the initial stage of loading ($0.25\varepsilon_y$). After that, differences between individual specimens were seen as the number of cycles increased. As indicated in Fig. 8 (b), the S-30 specimen showed an increase in strain rate of J2 larger than that of J3 in the $0.50\varepsilon_y$ cyclic loading; it then showed the opposite strain rate increase in $0.75\varepsilon_y$, a reversal of the slope in zone 1. After that, the same slope reversal phenomenon was observed in zone 2 ($0.75\varepsilon_y$ cyclic stress) and zone 3 ($0.9\varepsilon_y$ cyclic stress). The same trend was observed in the S-24, M-24, M-30, and M-50 specimens.

On the other hand, as can be seen in Fig. 8(h), the M-70 specimen showed the same slope reversal phenomenon (bond stress degradation, bond failure) as that of the S-30 specimen in zone 1 due to the difference in strain rate increase; this reversal did not appear in zone 2 or zone 3. The S-50 and S-70 specimens showed the same trend as the M-70 specimen. The reason for this is that, as explained in Sect. 3.1, bond deterioration of rebar and concrete in the joint core region progresses gradually from the tensile region to the compression region.

The quantitatively calculated bond stress distributions are shown in Fig. 9 and Table 4 to verify the evolution of the bond stress in each zone (zone 1, 2, and 3). The bond stress was calculated from the difference in strain in each zone, as shown in Eq. (1). As shown in Fig. 9 (b), the S-30 specimen exhibited a bond stress of 4.29 MPa at a $0.25\varepsilon_y$ applied load cycle in zone 1, which is close to the tensile side of the joint core region. At the same point in time, the bond stresses in zone 2, the center of the core region, and zone 3, close to the compression side, were 0.78 MPa and 2.31 MPa, respectively, about 82% and 46% lower than that in zone 1. Then, at $0.5\varepsilon_y$, the bond stress in zone 1 increased to 5.76 MPa, which is low, but, in zone 2 and zone 3, it increased to 1.51 MPa and 6.16 MPa, which are high values. At $0.75\varepsilon_y$, the bond stresses in zone 1 and zone 2 were 4.50 MPa and 1.20 MPa, respectively, lower than in the previous loading cycle; however, the bond stress in zone 3 increased to 8.83 MPa. At $0.9\varepsilon_y$, which is just before the yield of longitudinal reinforcing bars, the bond stress in zone 3 was 7.50 MPa, which was lower than in the previous loading cycle.

In contrast, the M-70 specimen exhibited the same levels of 1.20 and 1.16 MPa in zone 1 and zone 2 at $0.25\varepsilon_y$, respectively; in zone 3, however, the value was about 80% lower, at 0.24 MPa. Then, at $0.5\varepsilon_y$, the bond stresses in zone 1 and zone 2 increased significantly to 3.29 and 5.47 MPa, respectively, but the bond stress in zone 3 showed a smaller increased. At $0.9\varepsilon_y$, where the bond stress decreases after the maximum bond stress of zone 1 is reached, zone 2 has a large increase of 16.8 MPa, and the bond stress of zone 3 has a small increase of 2.66 MPa. The bond stresses of zones 2 and 3 did not decrease in subsequent load cycles. Based on these experimental results, this study concluded that the bond stress in zone 2, which is the center of the joint core

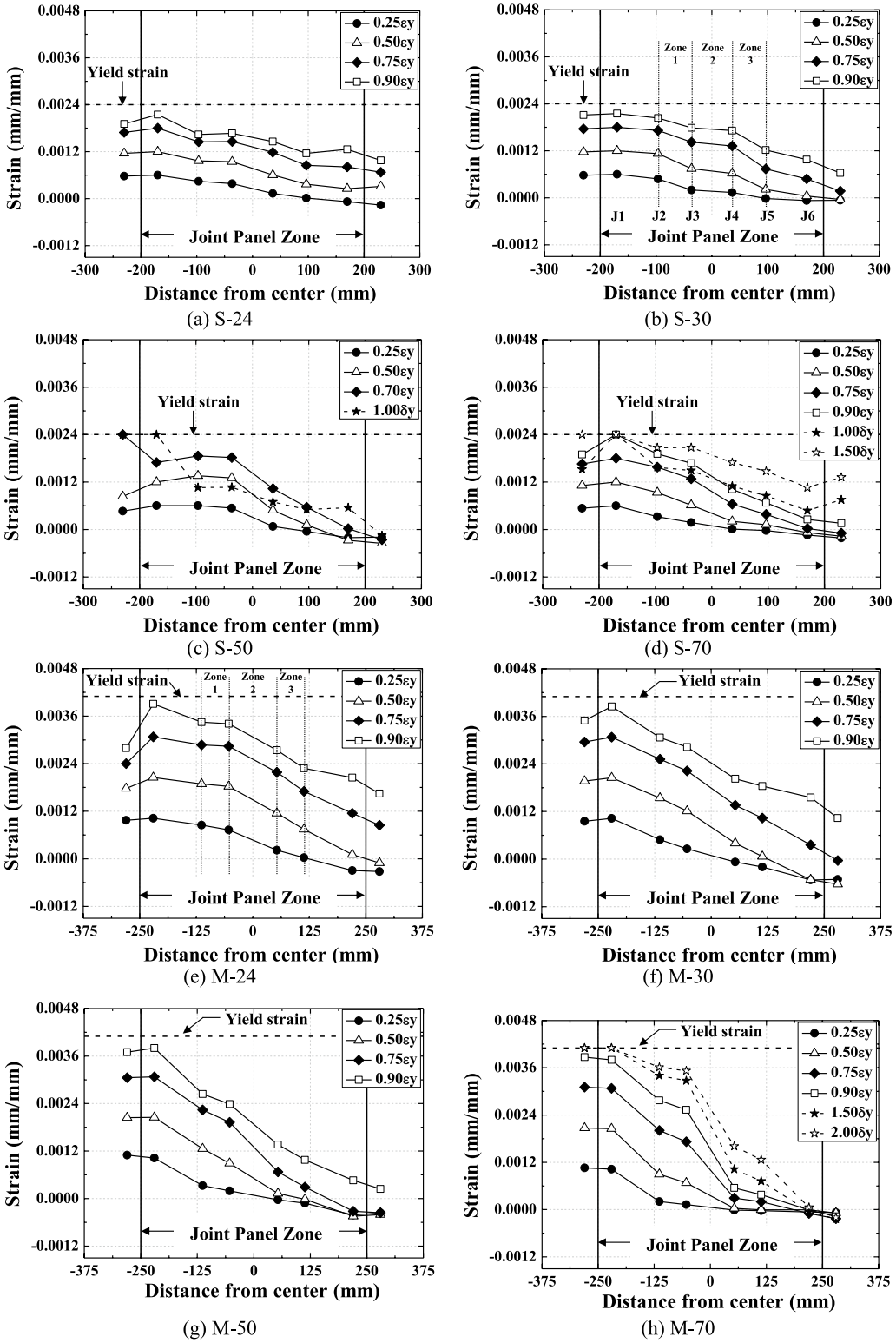

Fig. 8 Strain distribution of beam longitudinal rebar in joint panel zone (positive direction)

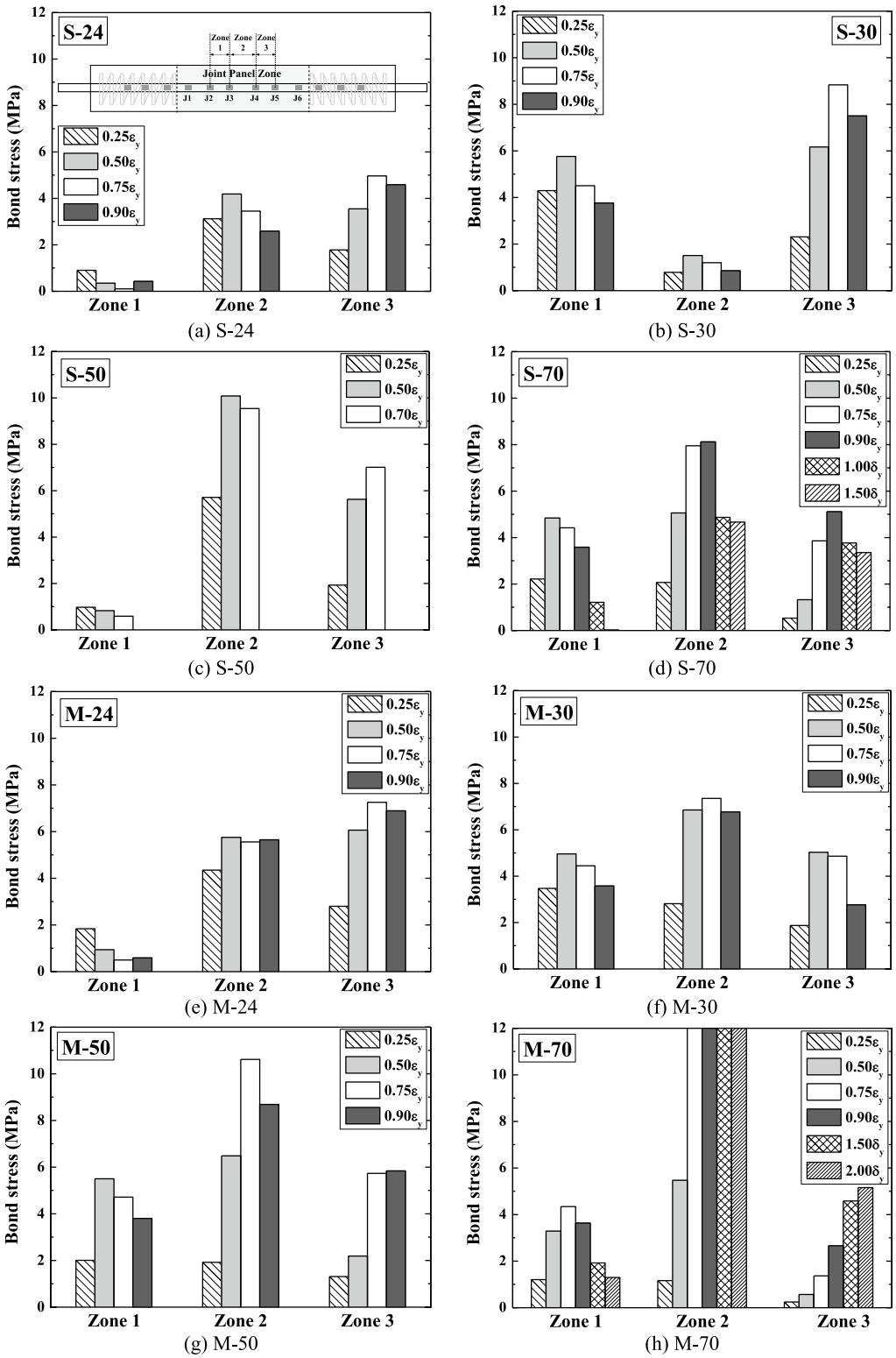

Fig. 9 Bond stress distribution each zone (positive direction)

Table 4 Bond stress for each region (positive direction)

Speci-mens	Bond stress (MPa)												Failure mode
	$0.25\varepsilon_y$			$0.50\varepsilon_y$			$0.75\varepsilon_y$			$0.90\varepsilon_y$			
	zone 1	zone2	zone3	zone 1	zone2	zone3	zone 1	zone2	zone3	zone 1	zone2	zone3	
S-24	0.90	3.12	1.78	0.35	4.18	5.55	0.10	3.45	4.97	0.43	2.59	4.59	Bond Failure
S-30	4.29	0.78	2.31	5.76	1.51	6.16	4.50	1.20	8.83	3.76	0.85	7.50	Bond Failure
S-50	0.97	5.91	1.93	0.83	10.1	5.63	0.59	9.54	7.00	–	–	–	Secure Bond
S-70	2.21	2.07	0.53	4.84	5.06	1.32	4.42	7.95	3.86	3.58	8.11	5.11	Secure Bond
M-24	1.84	4.35	2.79	0.93	5.75	6.06	0.49	5.55	7.25	0.59	5.64	6.89	Bond Failure
M-30	3.47	2.81	1.87	4.96	6.85	5.03	4.44	7.35	4.86	3.57	6.77	2.84	Bond Failure
M-50	2.00	1.92	1.31	5.50	6.48	2.19	4.71	10.6	5.73	3.80	8.68	5.83	Bond Failure
M-70	1.20	1.16	0.24	3.29	5.47	0.56	4.34	12.1	1.37	3.63	16.8	2.66	Secure Bond

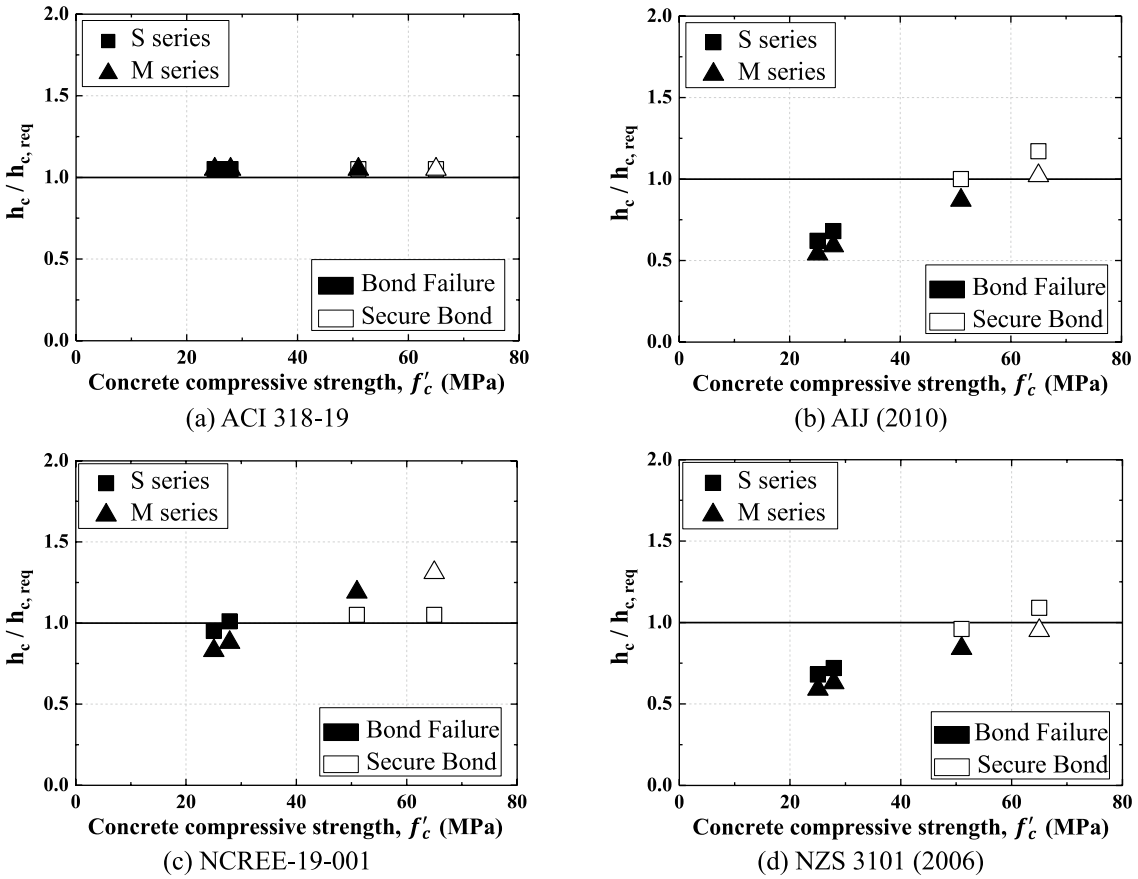

Fig. 10 Relationship of concrete compressive strength (f_c') and required column depth ratio ($h_c/h_{c,req}$)

region before the yielding of the beam longitudinal rebar, decreased after reaching the maximum bond stress. The 14th column of Table 4 shows the bond failure status of all the experimental specimens.

5 Proposal of Basic Bond Strength Equation

5.1 Evaluation of Existing Equations for Required Column Depth

As explained in Chapter 1, the column width ($h_{c.req}$) required by the current concrete design standards, shown in Table 1, is defined in various ways, including a simple definition based on the yield strength of the longitudinal rebar and a definition based on the assumption that the bond strength (τ_u) is greater than the bond stress (τ_f) caused by bending, as shown in Eq. (4). The ratio of required column width ($h_c/h_{c.req}$) according to concrete compressive strength (f'_c) is shown in Fig. 10 to evaluate whether the required column width is suitable according to the existing criteria. Here, h_c refers to the column width applied to the experiment in this study, and $h_{c.req}$ refers to the required column width presented in the existing criteria. If $h_c/h_{c.req}$ is greater than 1, the bond is a "Secure bond;" if it is less than 1, "Bond failure" is indicated. The results of the experiment were used to indicate type of destruction, and whether the bond failed or not, as determined in Sect. 3.2.

$$\tau_f < \tau_u \tag{4}$$

As shown in Fig. 10 (a), the American ACI 318–19 standard does not reflect the influence of concrete compressive strength, resulting in a constant required column width ratio, and does not adequately predict the results of all specimens. The Taiwanese NCREE-19–001 standard adequately predicts the secure bond specimen, but not the bond failure specimen (Fig. 10 (c)). AIJ (2010) in Japan and NZS 3101 (2006) in New Zealand provide more adequate predictions than those of the other standards, but were found to be less suitable for high strength concrete (Fig. 10 (b), (d)). These results indicate that the required bond length of beam longitudinal rebar penetrating the internal beam-column joints is strongly influenced by the concrete compressive strength, and it is necessary to propose a bond strength equation based on the concrete compressive strength.

5.2 Proposed Bond Strength Based on Concrete Compressive Strength

As shown in Table 1, bond strength is an important factor in determining the required column depth at the joint. In Japan's AIJ (2010), the bond strength (τ_u) is proportional to the 2/3 power of the concrete compressive strength, as based on experimental results that reflect the stress characteristics of the interior beam-column joints. However, these results were calculated based on a small number of experiments and show low suitability for high-strength concrete, as shown in Fig. 10 (b). Based on regression analysis, New Zealand's NZS 3101 (2006) uses the database of interior beam-column joint member experiments performed in previous studies to show that bond strength is proportional to the 1/2 power of the concrete compressive strength. In addition, as shown in Fig. 11, results derived using the existing criteria are somewhat higher than the bond strength calculated from the experimental results, resulting in an overestimation. For this reason, to more accurately predict the bond strength of beam-column joints, a regression analysis applying the experimental results of this study was conducted to reflect the influence of concrete compressive strength. The experimental data used in the regression analysis included the"Secure bond"specimen. Figure 12 shows regression analysis results indicating that the bond

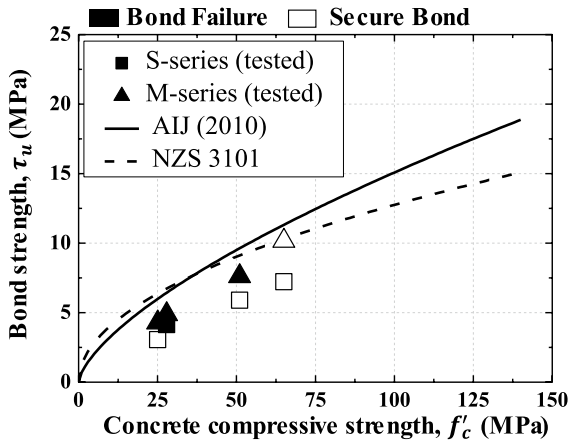

Fig. 11 Comparison of existing design criteria and test results

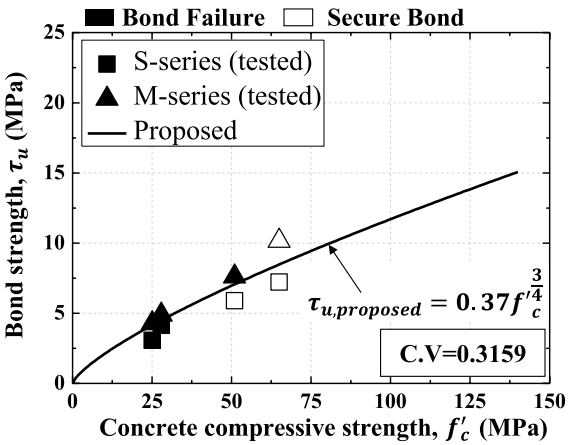

Fig. 12 Prediction of bond strength using proposed equation

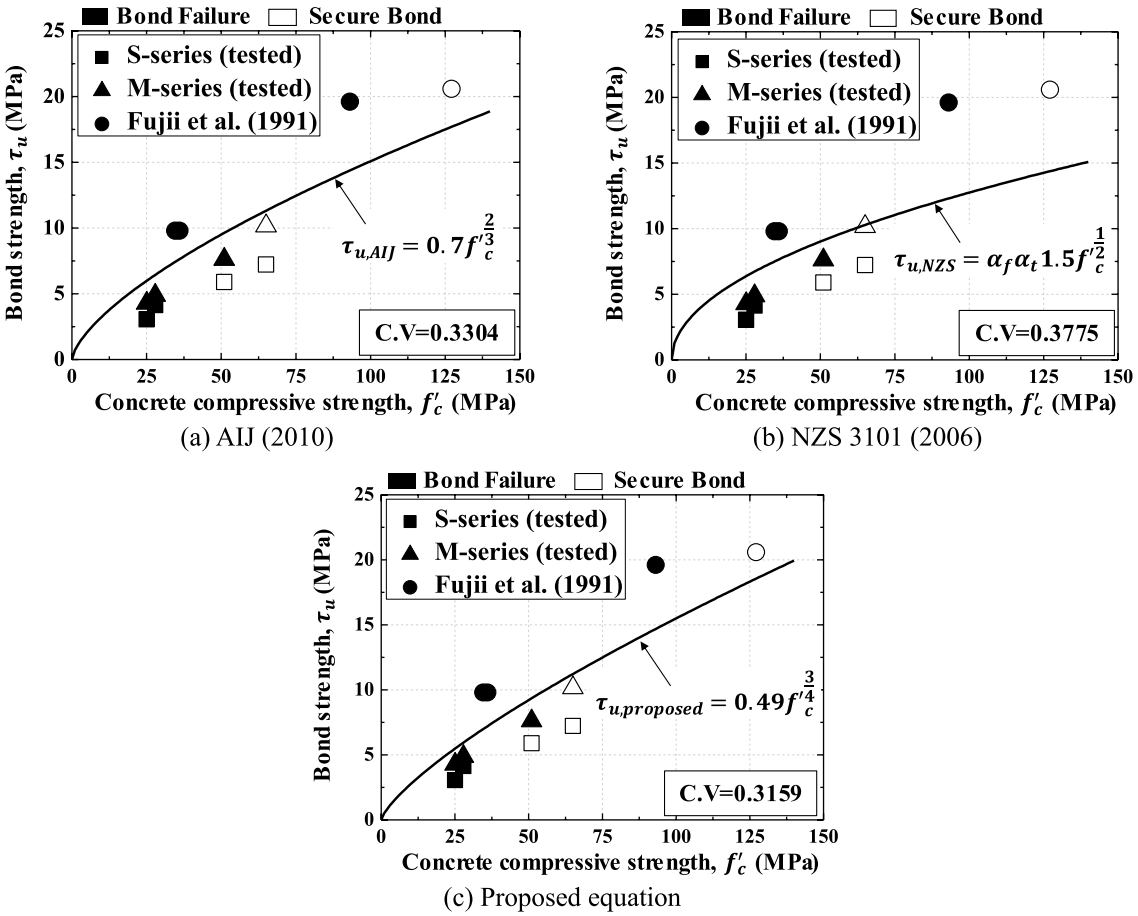

Fig. 13 Comparison of bond strength equation by concrete compressive strength

Table 5 Comparison of proposed equation and test results at maximum bond stress

Specimens		τ_{test}(MPa)	τ_{pro}(MPa)	τ_{AIJ}(MPa)	τ_{NZS}(MPa)	$\frac{\tau_{test}}{\tau_{pro}}$	$\frac{\tau_{test}}{\tau_{AIJ}}$	$\frac{\tau_{test}}{\tau_{NZS}}$
Tested in this study	S-24	3.06	5.49	6.00	6.38	0.56	0.51	0.48
	S-30	4.14	5.95	6.44	6.74	0.70	0.64	0.62
	S-50	5.89	9.35	9.63	9.11	0.63	0.61	0.65
	S-70	7.22	11.2	11.3	10.3	0.64	0.64	0.70
	M-24	4.28	5.49	6.00	6.38	0.78	0.71	0.67
	M-30	4.89	5.95	6.44	6.74	0.82	0.76	0.73
	M-50	7.61	9.35	9.63	9.11	0.81	0.79	0.84
	M-70	10.2	11.2	11.3	10.3	0.91	0.90	0.99
Fujii et al (1991)	Fujii 1	9.80	6.99	7.43	7.50	1.40	1.32	1.31
	Fujii 2	16.6	14.7	14.4	12.3	1.33	1.36	1.59
	Fujii 3	9.80	7.21	7.64	7.66	1.36	1.28	1.28
	Fujii 4	20.6	18.6	17.7	14.4	1.11	1.16	1.43
Average						0.92	0.89	0.94
Coefficient of Variation (%)						31.6	33.0	37.8

τ_{pro} = proposed equation of this study; τ_{AIJ} = design criteria equation of AIJ (2010); τ_{NZS} = design criteria equation of NZS

strength is proportional to three-quarters of the compressive strength of concrete, unlike the current standard. Furthermore, using the data of Fujii et al. (1991), who conducted experiments similar to this study, an expression for the bond strength in relation to the compressive strength of concrete was proposed as shown in Eq. (5).

$$\tau_{u.propose} = 0.49 f'^{\frac{3}{4}}_{c} \quad (5)$$

As can be seen in Fig. 13, the proposed bond stress equation predicts an experimental value similar to the existing criteria, with a coefficient of variation of 31.6%. However, as shown in Table 5, the ratio of the experimental value to the predicted bond strength was close to 1.0, with an average of 0.92; however, some differences occurred. This is because the bond characteristic of the joint is closely related to the compressive strength of the concrete, but it is affected by various parameters such as axial load ratio of column and yield strength of beam longitudinal rebar.

6 Conclusion

To directly investigate the effect of concrete compressive strength on bond characteristic at interior beam-column joints, this study was conducted by simulating the stress state of the joints under cyclic loading; the following conclusions were drawn.

(1) It was verified that the bond test method implemented by considering the stress state of the interior beam-column joint under cyclic loading is an appropriate method to identify the bond characteristic of beam longitudinal rebar.
(2) In the case of a specimen with bond failure, the bond stress in the core region of the joint was found to increase due to the bond stress-slip relationship, with the bond stress between the rebar and concrete first disappearing in the tensile area (Local CL) and then transferring to the compressive area (Local CR). After reaching the maximum bond stress in each section, the amount of slippage increased significantly, indicating the occurrence of pinching.
(3) Through the strain rate and bond stress distribution of beam longitudinal rebar, after reaching the maximum bond stress in each zone, the bond stress degraded due to the reversal of strain rate in the applied loading cycle (zones 1, 2, and 3), and the bond failure was judged according to the presence or absence of bond stress degradation in the center of the joint core region (zone 2).
(4) The maximum bond stress of the joint showed a tendency to increase with the increase in the compressive strength of concrete, and a bond strength equation for concrete compressive strength was proposed based on the experimental results reflecting the bond characteristics. It was confirmed that the proposed bond strength is proportional to the 3/4th power of the compressive strength of the concrete, which is similar to the experimental values; however, it was necessary to additionally consider various parameters such as the axial load ratio of the column, the yield strength of the reinforcing bar, and the diameter. We also plan to conduct further research in the future with experiments at the member level.

Acknowledgements
Not applicable.

Author contributions
M. Jo: data curation, investigation, project administration, visualization, writing—original draft, H. Kim: conceptualization, methodology, D. Kim: formal analysis, S. Lim: formal analysis, Y. Choi: data curation, J. Lee: methodology, K. Kim: conceptualization, funding acquisition, project administration, supervision, writing—review and editing. All authors have read and agreed to the published version of the manuscript.

Funding
This work was supported by the National Research Foundation of Korea(NRF) grant funded by the Korea government(MSIT) (2023R1A2C3002443); This research was supported by Basic Science Research Program through the National Research Foundation of Korea(NRF) funded by the Ministry of Education (2019R1A6A1A03032988); This research was supported by Basic Science Research Program through the National Research Foundation of Korea(NRF) funded by the Ministry of Education (RS-2023–00239201); This research was supported by Korea Basic Science Institute (National research Facilities and Equipment Center) grant funded by the Ministry of Education (RS-2022-NF000835); This work was supported by the research grant of Kongju National University in 2025.

Availability of Data and Materials
Some or all data, models, or code that support the findings of this study are available from the corresponding author upon reasonable request.

Declarations

Ethics Approval and Consent to Participate
All authors of the manuscript confirm the ethics approval and consent to participate following the Journal's policies.

Consent for Publication
All authors of the manuscript agree on the publication of this work in the International Journal of Concrete Structures and Materials.

Competing Interests
The authors declare that they have no competing interests.

Author details
[1]Department of Architectural Engineering, Kongju National University, Gongju, Republic of Korea. [2]Department of Green Smart Architectural Engineering, Kongju National University, Gongju, Republic of Korea. [3]Department of Architectural Engineering, Kongju National University, Cheonan, Republic of Korea. [4]Division of Structural Business, East structures, Cheonan, Republic of Korea. [5]School of Civil, Architectural Engineering and Landscape Architecture

Sungkyunkwan University, Suwon, Republic of Korea. [6]Department of Green Smart Architectural Engineering and Urban Systems Engineering, Kongju National University, Cheonan, Republic of Korea.

Received: 17 March 2025 Accepted: 6 June 2025
Published online: 27 August 2025

References

ACI (American Concrete Institute). (2019). Building Code Requirements for Structural Concrete and Commentary, ACI 318–19. Farmington Hills, MI: ACI

AIJ (Architectural Institute of Japan). (2010). AIJ standard for structural calculation of reinforced concrete structures. Tokyo: AIJ

Alva, G. M. S., El Debs, A. L. H., de Cresce, El., & Debs, M. K. (2007). An experimental study on cyclic behavior of reinforced concrete connections. *Canadian Journal of Civil Engineering, 34*, 565–575. https://doi.org/10.1139/l06-164

ASTM. (2021). Standard test method for compressive strength of cylindrical concrete specimens. ASTM C39/C39M-21. West Conshohochen, PA: ASTM 2021

Brooke, N. J., Megget, L. M., & Ingham, J. M. (2006). Bond performance of interior beam-column joints with high-strength reinforcement. *ACI Structural Journal, 103*(4), 596–603. https://doi.org/10.1435/16436

Fujii, S., Murakami, H., Yamada, T., & Morita, S. (1991). Bond properties of beam through bars in high-strength reinforced concrete beam-column joints. *Proceedings of the Japan Concrete Institute, 13*(2), 483–488.

Hakuto, S., Park, R., & Tanaka, H. (1999). Effect of deterioration of bond of beam bars passing through interior beam-column joints of flexural strength and ductility. *ACI Structural Journal, 96*(5), 858–864. https://doi.org/10.1435/740

Hong, S. G., Lee, S. G., & Kang, T. H. K. (2011). Deformation-based strut-and-tie model for interior joints of frames subject to load reversal. *ACI Structural Journal, 108*(4), 423–433. https://doi.org/10.1435/51682982

Hwang, H. J., Eom, T. S., & Park, H. G. (2015). Bond-slip relationship of beam flexural bars in interior beam-column joints. *ACI Structural Journal, 112*(6), 827–837. https://doi.org/10.1435/51687708

Karayannis, C. G., & Chalioris, C. E. (2013). Shear tests of reinforced concrete beams with continuous rectangular spiral reinforcement. *Construction and Building Materials, 46*, 86–97. https://doi.org/10.1016/j.conbuildmat.2013.04.023

Kitayama, K., Otani, S., & Aoyama, H. (1987). Earthquake resistant design criteria for reinforced concrete interior beam-column joints. *Pacific Conference on Earthquake Engineering, 1*, 315–326.

Lee, H. J., Chen, H. C., & Tsai, T. C. (2018). Simplified design equation of minimum interior joint depth for special moment frames with high-strength reinforcement. *Int J Concr Struct Mater, 12*(70), 1–15. https://doi.org/10.1186/s40069-018-0303-2

Lee, J. Y., Kim, J. Y., & Oh, G. J. (2009). Strength deterioration of reinforced concrete beam-column joints subjected to cyclic loading. *Engineering Structures, 31*(9), 2070–2085. https://doi.org/10.1016/j.engstruct.2009.03.009

Lee, S., Kitayama, K., Otani, S., & Aoyama, H. (1992). Shear strength of RC interior beam-column joints using high strength materials. *Trans. Jpn. Concr. Inst., 14*(2), 379–384.

Leon, R. T. (1989). Interior joints with variable anchorage lengths. *Journal of Structural Engineering, ASCE, 115*(9), 2261–2275. https://doi.org/10.1061/(ASCE)0733-9445(1989)115:9(2261)

Meinheit D. F. and Jirsa J. O.(1977). Shear Strength of Reinforced Concrete Beam-Column Joints, Report No. 77–1, Department of Civil Engineering, Structures Research Laboratory, University of Texas at Austin, TX

NCREE. (2019). Design Guideline for Building of High-Strength Reinforced Concrete Structures (Draft) (NCREE-19–001). Taipei, Taiwan: National Center for Research on Earthquake Engineering;.

NZS 3101. (2006). Concrete structures standard part 1-the design of concrete structures, Wellington. Standards New Zealand: New Zealand

Sadjadi, R., Kianoush, M. R., & Talebi, S. (2007). Seismic performance of reinforced concrete moment resisting frames. *Engineering Structures, 29*(9), 2365–2380. https://doi.org/10.1016/j.engstruct.2006.11.029

Publisher's Note

Min-Su Jo Research Assistant Professor, Department of Architectural Engineering, Kongju National University, Republic of Korea

Hyeong-Gook Kim Associate Professor, Department of Green Smart Architectural Engineering, Kongju National University, Republic of Korea

Dong-Hwan Kim Research Assistant Professor, Department of Architectural Engineering, Kongju National University, Republic of Korea

Su-A Lim Research Assistant Professor, Department of Architectural Engineering, Kongju National University, Republic of Korea

Yun-Soo Choi Graduate student, Department of Architectural Engineering, Kongju National University, Republic of Korea

Jung-Yoon Lee Professor, School of Civil, Architectural Engineering and Landscape Architecture Sungkyunkwan University, Republic of Korea

Kil-Hee Kim Professor, Department of Green Smart Architectural Engineering & Urban Systems Engineering, Kongju National University, Republic of Korea